Advances in Concrete Construction, *Vol. 9, No. 3* (*2020*) *257-265*
DOI: https://doi.org/10.12989/acc.2020.9.3.257

Algorithms to measure carbonation depth in concrete structures sprayed with a phenolphthalein solution

Christian C. Ruiz*, José L. Caballero[a], Juan H. Martinez[b] and Willian A. Aperador[c]

Department of Mechatronic Engineering, Universidad Militar Nueva Granada, Carrera 11 #101-80, Colombia

(*Received September 18, 2019, Revised December 3, 2019, Accepted January 23, 2020*)

Abstract. Many failures of concrete structures are related to steel corrosion. For this reason, it is important to recognize how the carbonation can affect the durability of reinforced concrete structures. The repeatability of the carbonation depth measure in a specimen of concrete sprayed with a phenolphthalein solution is consistently low whereby it is necessary to have an impartial method to measure the carbonation depth. This study presents two automatic algorithms to detect the non-carbonated zone in concrete specimens. The first algorithm is based solely on digital processing image (DPI), mainly morphological and threshold techniques. The second algorithm is based on artificial intelligence, more specifically on an array of Kohonen networks, but also using some DPI techniques to refine the results. Moreover, another algorithm was developed with the purpose of measure the carbonation depth from the image obtained previously.

Keywords: carbonation; concrete; phenolphthalein; Kohonen network; artificial intelligence; image processing

1. Introduction

The service life of concrete structures with reinforced steel is commonly calculated according to its compressive resistance; however, several factors can cause the structure to deteriorate prematurely (Wang and Yao 2018). Since the reinforced concrete is extensively used in construction, it is important to acknowledge the corrosion of steel as the main cause of the reduction in service life by producing cracks in the structure, carbonation being the means whereby this phenomenon took place (Zambon *et al*. 2018).

The use of concrete history shows that failure cases due to mechanical loads are minimal, hence concrete structures problems are frequently related to corrosion steel. Even with the acquired experience of designers, the carbonation process and corrosion keep being cases of study always looking for avoiding them (Malerba *et al*. 2017). Besides, carbonation is produced in environments with high CO_2 concentration; therefore, the main structures that are affected are bridges and park buildings (Papadakis 2013, Rodriguez *et al*. 2014).

The carbonation process is a phenomenon present in concrete structures that happens naturally through a chemical reaction between some concrete components and the carbon dioxide presents in the environment (Wang and Lee 2019). This phenomenon implies a potential risk that can significantly affect the resilience of the structure (Akcay *et al*. 2016, Barros, *et al*. 2013), since, if the carbonation depth reaches the steel reinforcement, the steel can suffer corrosion, which in turn can mean more serious problems such as deformation or stability problems in the structure (Zhou *et al*. 2019, Zhu and Francois 2013). From a chemical point of view, the steel must be in a basic pH normally 12, although it can be considered in an optimal condition provided that it is not less than 11.5 (Pu *et al*. 2017). At the moment the carbonation takes effect, its pH starts to decrease until 9 or even less causing the problems mentioned above (Jiang *et al*. 2017). Even though many techniques have been applied in order to avoid carbonation (Woyciechowski and Soko 2017), several potentially dangerous buildings must be analyzed, either by they are very old construction or by a lack of technical data (Cao and Ronagh 2013).

The most traditional way to carry out the study is to extract a sample from the concrete column, and then apply phenolphthalein in its transversal section, in this way the sample will turn a totally pinkish color if the structure does not have carbonation problems or, on the contrary, only the parts that are in good condition will turn that color (Tang *et al*. 2018). As can be seen in Fig. 1, the process to measure the depth of carbonation is done manually by measuring the carbonated zone through any measuring instrument, which can lead to mainly human errors since this process is not usually done accurately and is often done subjectively. Therefore, digital image processing together with artificial intelligence can solve these problems and ensure the most correct carbonation profile measurement.

Artificial intelligence arises from the need to give machines the ability to learn from their environment based on biological concepts specific to the human being (Antonio

*Corresponding author, Researcher
E-mail: u1802566@unimilitar.edu.co
[a]M.Sc.
E-mail: jose.caballero@unimilitar.edu.co
[b]Researcher
E-mail: juan.martinez@unimilitar.edu.co
[c]Ph.D.
E-mail: william.aperador@unimilitar.edu.co

ISSN: 2287-5301 (Print), 2287-531X (Online)

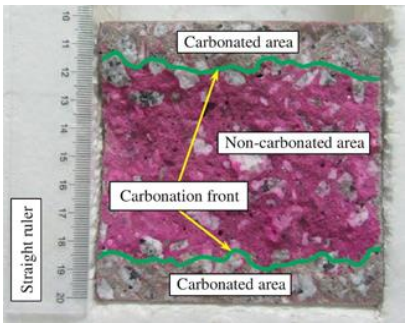

Fig. 1 Carbonation measurement applying phenolphthalein solution

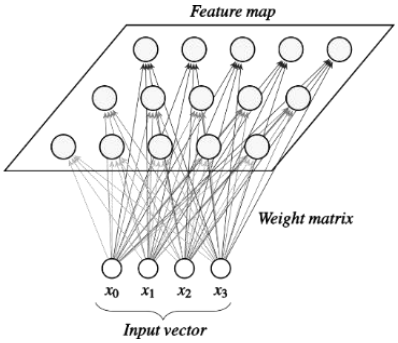

Fig. 2 Scheme of Kohonen self-organizing maps

et al. 2018, Makridakis 2017), for instance, an autonomous robot can be endowed with practically absolute knowledge, but if in practice the robot operates in an unknown environment the knowledge given will not be useful if it is not capable of adapting to the new environment (Tetta 1986). From the above, artificial intelligence have three broad areas of study: fuzzy logic, neural networks and genetic algorithms (Shibata *et al.* 1993), all of them imply a set of algorithms capable of operating in various unplanned environments, whereas maintaining a high level of efficiency.

In this study, it is proposed to use a Kohonen self-organizing map (KSOM), which is an unsupervised learning neural network. These kinds of neural networks are based on a specific aspect of the human being. In this case, self-organizing maps are inspired by the brain's ability to recognize and group the most significant traits of the environment captured through its sensory organs (sight, hearing, etc.) (D'Urso *et al.* 2019). The application of this neural network consists of the reduction of the dimensionality of the data of a high dimension (third dimension up to n-dimensions) in a two-dimensional map (Ali Hameed *et al.* 2019) or some cases one-dimensional, and to cluster the data forming groups. It is a model consisting of two layers, an input layer and a processing layer. The input layer receives the information from the input vector, in Fig. 2 it corresponds to the input vector [$x1$ $x2$ … xn], in this case, would be up to $x3$. The processing layer is fully connected to the input layer via synaptic weights, just like the conventional neural network.

2. Algorithm development

Table 1 Properties of the experimental database

Features	# Samples	Reference
Circular Samples Carbonation depth available. Accelerated carbonation. Different elapsed times. Concrete with fly ash.	84	(Zhuguo and Sha 2018)
Rectangular samples. Portland-fly ash cement.	5	(Revert *et al.* 2018)
Rectangular samples. Accelerated carbonation. Portland cement (type P.II 52.5). Different elapsed times.	9	(Liwu *et al*. 2017)
Rectangular samples. Carbonation depth available. Different elapsed times. Portland cement.	8	(Guedes *et al*. 2018)
Rectangular samples. Natural carbonation. Carbonation depth available.	16	(Emmanuel *et al.* 2009)
Rectangular samples. Portland cement with different % of fly ash. Accelerated carbonation. Carbonation depth available.	4	(Xu *et al.* 2010)
Rectangular samples. Different mix proportion. Portland slag cement.	4	(Taffese *et al.* 2015)
Rectangular samples. Portland cement.	1	(Paul *et al.* 2018)

In order to verify the validity of the implemented algorithms, a database of concrete specimens was obtained to which the phenolphthalein test was applied. This database was obtained from several articles, detailed in Table 1. In the database, there are tests with a high degree of variation among them, with different forms in the test tube, different image qualities, different light conditions, concrete with different aggregates and even some with a thymolphthalein test (pH indicator substance similar to phenolphthalein). There are 131 images.

2.1 KSOM training

The operation of neural networks requires two phases, the first of training and the second of operation. The training consists of three stages, competitive phase, cooperative phase and adaptive phase.

2.1.1 Competitive phase

In the competitive phase, the distance between the input vector and the weight vector of each neuron is calculated, taking into account that the weights are randomly initialized in a coherent range. The size of the weight vector of each neuron is the same as the size of the input data (Khvorostukhina *et al.* 2017). The computation of distance can be calculated in several ways, depending on the origin of the input data. In general, it can be calculated as the Euclidean distance, Eq. (1).

$$D(P,Q) = \sqrt{\sum_{i=1}^{n}(P_i - Q_i)^2} \quad (1)$$

With all distances, the neuron with the shortest distance is selected, and this is the winning neuron of the competitive phase. For the implementation, although the calculation of the Euclidean distance is not complex, the square root is not computed since it does not alter the magnitude of the measurements, and the smaller distance will remain the smaller even without the root and the computational cost will be reduced.

2.1.2 Cooperative phase

In this phase, the term neighborhood function arises. The neighborhood function determines the effect of the change in the weights of neurons close to the winning neuron in each iteration of the training. At the beginning of the training, all neurons on the map are affected, but as the iterations progress, the range of the neighborhood function decreases (Hikawa and Maeda 2015). The decreasing function used is the Gaussian function, Eq. (2).

$$f(x) = a * exp^{-\frac{(x-b)^2}{2*c^2}} \quad (2)$$

In Eq. (2), '*a*' is the value of the highest point of the bell, '*b*' is the position of the center of the bell, and '*c*' controls the width of the bell, these three terms are constant values, although '*c*' becomes a variable in the implementation of this function with the Kohonen network. Taking this equation as a basis, a value '*a*' of 1 is used since the total effect of the winning neuron is 1 and as it moves away through neighboring neurons this value should decrease. The constant '*b*' is 0 because the center of the bell will always be the winning neuron and the parameter '*x*' will always depend on the winning neuron, which is the center (Moshfe *et al.* 2010). At the beginning, '*c*' is a constant that controls the width of the bell and it was mentioned before that the width of the bell must be reduced with the increase of iterations, hence, for its implementation, this value must become a variable σ. For this purpose, a decreasing exponential function is used that depends on the iterations '*k*', as can be seen in Eq. (3)-(4).

$$\sigma(\mathrm{k}) = \sigma_0 * exp^{-(k/\tau_1)} \quad (3)$$

$$\tau_1 = 1000/\log(\sigma_0) \quad (4)$$

According to Eqs. (3)-(4), τ_1 is a time constant and σ_0 is the start value function. Thus, the Gaussian neighborhood function $h(k)$ (Eq. (5)) is as follows

$$h(k) = exp^{-\left(\frac{d^2}{2\sigma^2}\right)} \quad (5)$$

"*d*" is the shape of the neighborhood function index distance between the winning neuron and its neighbors, giving a growing value to each zone according to its distance from the winning neuron. This whole process corresponds to soft competitive learning, in which the winning neuron and its neighbors receive training. It is also possible to implement strong competitive learning, where only the winning neuron receives the training and therefore it would not be necessary to implement a neighborhood function. Soft competitive learning resembles in a greater proportion of the biological functioning of the brain than strong competitive learning (Cheng *et al.* 2006).

2.1.3 Adaptive phase

In the adaptive phase, the synaptic weights are updated for each neuron according to the scope of the neighborhood function. For a two-dimensional map, the synaptic weights are updated following Eqs. (6)-(7).

$$w_{ij}(k+1) = w_{ij}(k) + \mu(\mathrm{k}) * \mathrm{h}_{ij}(k) * (x - w_{ij}(k)) \quad (6)$$

$$\mu(\mathrm{k}) = \mu_0 * exp^{-(k/\tau_2)} \quad (7)$$

μ is the learning factor and determining how fast the algorithm advances with each iteration, a large factor will make the network train faster, but it will be more susceptible to being unstable. Its constant parameters are typically taken as μ0=0.1 *y* τ2=1000. As the neighborhood function, the learning factor also decreases with iterations (Li *et al.* 2011). The training must repeat the competitive, cooperative and adaptive phases, and is terminated when the algorithm reaches a number of maximum iterations determined a priori or when the synaptic weights no longer change.

2.2 Arrangement of Konohen networks

This algorithm is composed of an array of two Kohonen networks working together. The first step in the implementation of KSOM is to perform exploratory data analysis by extracting representative characteristics of non-carbonate zones (NCZ) and carbonate zones (CZ) from the 131 images in the database.

2.2.1 Exploratory data analysis

The first process of the algorithm consists of carrying out the training of the network, specifically the output layer of the network is a two-dimensional map.

Owing to this algorithm works with color images, it is proposed to work with images in an HSV color model instead of the RGB model. Fig. 3 shows an example of the transformation of the color model. In the RGB model, two distinguishable zones were recognized, the concrete zone and the phenolphthalein-marked zone. In the HSV model, there is a new zone (marked with a black circle) that normally surrounds the NCZ but corresponds to a CZ.

The training is carried out by extracting significant samples from all the images present in the database. In this training it is important to recognize when to finish it because there is no automatic parameter or rule that allows stopping the training by the program, you must observe the data and finish it when the data are well distributed along

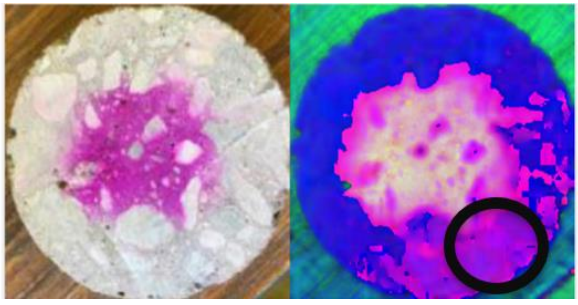

Fig. 3 Color model change from RGB to HSV

Fig. 4 Exploratory data analysis for 30x30 network

Fig. 5 Clustering result

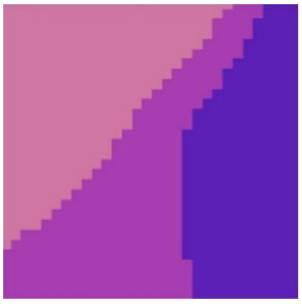

Fig. 6 Two-dimensional map labeling

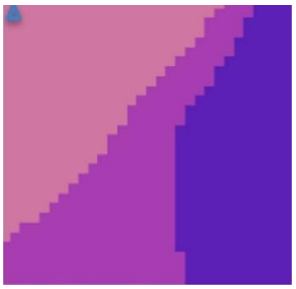

Fig. 7 The supervised phase of the Kohonen network

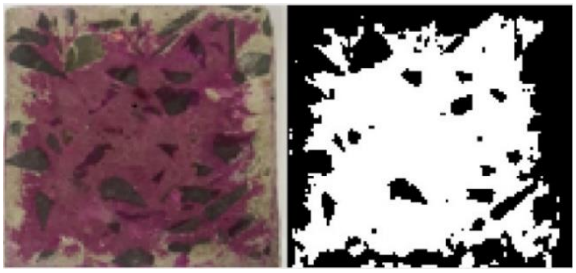

(a) Comparison between initial and final image

(b) The result of the KSOM algorithm

Fig. 8 Kohonen network output

with the map always avoiding overtraining. In this case, 418 iterations were used, see Fig. 4.

2.2.2 Clustering

In this stage, it is necessary to indicate to the algorithm how many groups it looks for in the map of the exploratory analysis of data, see Fig. 4. As mentioned before, owing to the change of color model, a new CZ zone appears that is considered similar to the NCZ. If only two groups are searched the KSOM will classify them in the same group, therefore there will be a group containing CZ and NCZ. In that case, the algorithm will not work, and its results will be deficient, hence in the Clustering stage, it is necessary to look for three groups, two of them will be NCZ and one CZ. Fig. 5 shows the three neurons once trained with the representative colors, which in turn correspond to the three groups mentioned.

2.2.3 Labeling

The next step is to label the map in Fig. 4, with the three clusters that were trained from Fig. 5. To this end, each neuron on the map was operated with the one-dimensional network (Fig. 5). In a new map, depending on the cluster in which it was clustered, the position of the neuron will acquire the weights of the cluster, see Fig. 6.

2.2.4 Supervised phase

Before setting up the network it is necessary to know which groups in the previous map that correspond to CZ and NCZ. Fig. 7 shows this procedure, where the network classifies a non-carbonate data entry in the upper left corner, hence this group will correspond to NCZ. It is not necessary to test the other two groups since there is only one non-carbonate group and the remaining groups are carbonate groups.

2.2.5 Commissioning

After this procedure, the network can be tested, only with the pixel data of the images performing the competitive phase of the training and check the position of the winning neuron in the map of Fig. 7. Then a new binary image is created where if this pixel corresponds to CZ, in the image will have a value of '1' and otherwise a value of '0'. Fig. 8(a) shows the result of the Kohonen network. Once the binary image has been obtained, applying diverse digital image processing techniques such as morphological operations, the contour drawn in Fig. 8(b) is obtained.

2.3 Algorithm DPI

This algorithm is based on the work done in (Jung *et al.* 2017), but extending the method to circular specimens. For circular specimens, the diagram in Fig. 9 is used. For square and rectangular specimens, it is only necessary to follow the

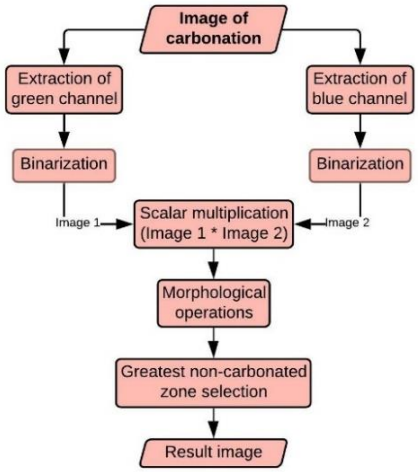

Fig. 9 DPI algorithm diagram

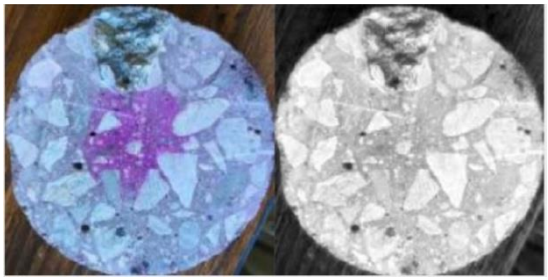

Fig. 10 Grayscale image extracting the B channel

extraction branch of the *G*-channel omitting the scalar multiplication step.

2.3.1 Grayscale

In order to obtain the grayscale image, only the *G* channel is extracted (green in the RGB model). In this way, the color information of the image is used to obtain a more suitable grayscale image than using a weighted average of the RGB channels. At the same time, the *B* channel is extracted to obtain a grayscale image where there is no NCZ, see Fig. 10.

2.3.2 Binarization

The main objective of this operation is to begin to differentiate the two zones that are in the image by the method of Otsu (Otsu 1979). This corresponds to the CZ and NCZ, respectively. In this way, a binary image will be obtained in which the pixels normalized in '1' will be CZ and the pixels in '0' will be NCZ, for the image extracting the channel *G*. For the image extracting the channel B, one zone is obtained for the test tube and another zone for the background, as illustrated in Fig. 11.

2.3.3 Morphological operations

In the next step, the images in Fig. 11 are multiplied scalarly. Once the image has been multiplied, morphological operations are applied to eliminate small areas erroneously marked, as shown in Fig. 12(a). In case there is more than one ZNC at this point, it is necessary to select the largest area and delete the other areas. Fig. 12(b) shows the result.

Fig. 11 Binarized result for image extracting channel B and channel *G*, respectively

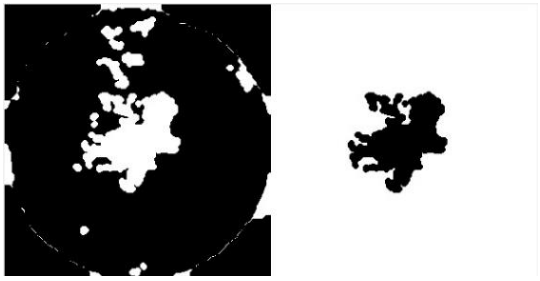

(a) Comparison before and after morphological operations

(b) Final result DPI algorithm

Fig. 12 DPI algorithm output

3. Carbonation depth measurement

This algorithm aims to calculate the magnitude of carbonation depth in the database images. To do this, the final binary images of the previously implemented algorithms are used. Fig. 13 shows the flow diagrams of the algorithms for circular and rectangular specimens, respectively.

3.1 Rectangular specimens

Fig. 14 will be used as an example to explain the algorithm, in this case, the border was drawn to see what the limit of the image is.

The algorithm consists of projecting a line from the edge of the image from each point of the edge to the center of the image. The pixels will be counted from the edge to the first black pixel found and the coordinate of this point is saved, this last procedure is done for each projected line. Fig. 15 clearly shows the procedure.

Although this type of measurement is not recommended for rectangular specimens because the depth of carbonation is usually measured according to Fig. 16. For this reason, the implementation of the algorithm to measure the depth of carbonation by a circular pattern is necessary for each

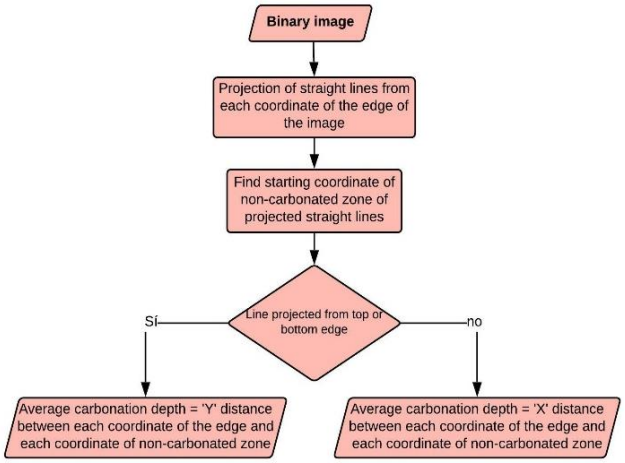

(a) Rectangular specimen

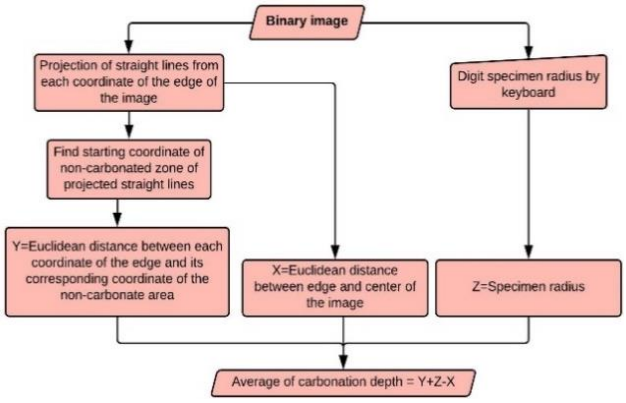

(b) Circular specimen

Fig. 13 Carbonation depth algorithms

Fig. 14 Binary image

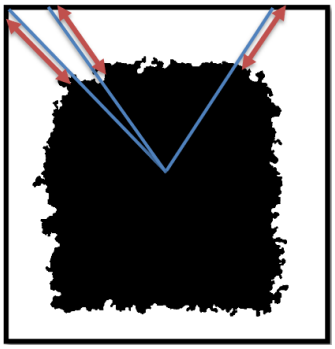

Fig. 15 Measurement of carbonation depth by means of a circular pattern

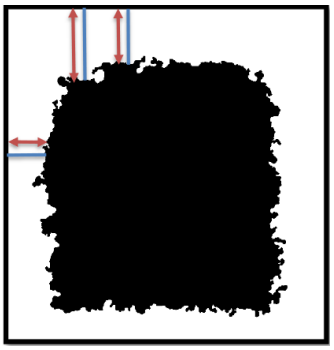

Fig. 16 Measurement of carbonation depth by means of a rectangular pattern

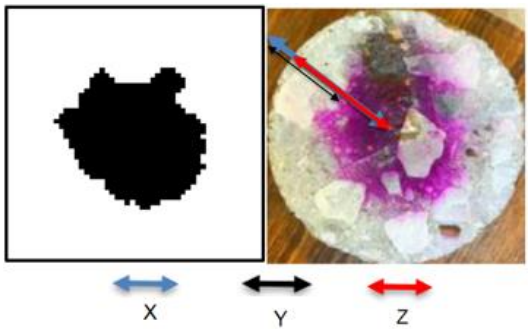

Fig. 17 Carbonation depth measurement in circular specimens

projected line to calculate the corresponding leg. Since we have the starting and ending point (x, y) for each line in Fig. 15, to obtain the equivalent measurement we only need to make the difference in 'y' from the starting point and endpoint for the projected upper and lower edge straight lines, and the difference in 'x' for the straight lines projected from the right and left edge.

It is important to mention that the measurement is made by using a circular pattern, although it requires an extra procedure, because computationally the rectangular pattern requires to recognize when to measure vertically and when to measure horizontally, while the circular pattern such recognition lies in recognizing which straight lines have been projected from the top and bottom edge and which from the right and left edge.

3.2 Circular specimens

In the case of circular specimens, the procedure is similar but in the resulting binary image, it is not possible to differentiate the background from carbonate concrete, as shown in Fig. 17.

In order to calculate the carbonation depth, it is necessary to have three data, which are detailed in figure 17. The data '*X*' is the length from the edge of the image to the center of it, this data is easy to obtain since each straight line is projected taking into account these two points,

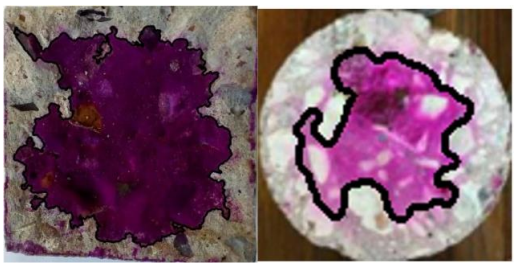

Fig. 18 Calculation of carbonation depth for square and circulating specimens

therefore, with the Pythagorean Theorem, it is possible to calculate this length. The data '*Y*' is the initial depth measured by the algorithm, the algorithm finds the initial point and the final point of this line, also through the Pythagoras theorem can know the length of the line. The data '*Z*' corresponds to the radius of the probe in pixels, which corresponds to half the size of the image. In this way, with the Eq. (6) we have the real carbonation depth (CB)

$$CB = Y + Z - X \tag{8}$$

Fig. 18 shows the result of the calculation of the carbonation depth for a square specimen and for a circular specimen. In the case of the square specimen, the carbonation depth in percent was 28.4% and in millimeters, it was 8.5 mm, considering a specimen of 60×60 mm. For the circular specimen, the result in the percentage was 45.1% and in millimeters, it was 11.41 mm, with a specimen of diameter 50 mm.

4. Results

Table 2 shows the results considering that the segmented non-carbonated zone coincides with the real zone in the test tube, in case it will be considered as a positive result.

From the above data, it can be inferred how the algorithm based on artificial intelligence obtained better results approximately 36.8% in rectangular test tubes, 9.53% in circular test tubes, and taking into account both test tubes 19.8%. It is important to highlight that, in the case of the PDI algorithm, an algorithm was implemented for rectangular specimens. For circular specimens, it was necessary to make some changes in the algorithm. In the algorithm based on artificial intelligence, the same algorithm works regardless of the specimen type.

In order to more accurately verify the quality of segmentation in the AI algorithm, an analysis is performed using Dice's Coefficients (DScore). In this way, it is possible to have a percentage that indicates the similarity between the image obtained by the algorithm and the ideal segmentation (Thada and Vivek Jaglan 2013). The ideal segmentation was obtained by manual segmentation of several images from the database. It is important to mention that the ideal segmentation may include errors because it was done manually, although it was done as objectively as possible.

Table 2 Comparison of results between the IA and DPI algorithm

Algorithm	% All positive outcomes	% Positive rectangular	% Positive circular
DPI	77.69%	71.70%	81.81%
IA	93.08%	98.11%	89.61%

Table 3 Quality of segmentation using DScore with the IA algorithm

IA	# Samples	AVG DScore
Rectangular	10	96.32%
Circular	12	97.93%
AVG	22	97.2%

Table 4 Quality of segmentation using DScore with DPI algorithm

DPI	# Samples	AVG DScore
Rectangular	10	94.43%
Circular	12	96.17%
AVG	22	95.38%

Table 5 Carbonation depth measurement results

Carbonation depth			Absolute error
%	mm	Theory (mm)	mm
9,4	4,7	6,3	1,6
25,9	13,4	7,2	6,2
22,9	11,5	7,1	4,4
20,9	10,4	7,6	2,8
3,7	0,9	0,0	0,9
41,4	10,5	11,0	0,5
31,3	7,8	11,0	3,2
21,7	5,4	5,0	0,4
55,4	14,0	15	1,0
17,1	4,3	3	1,3
38,1	9,6	10	0,4
47,6	12,0	14	2,0
50,4	12,7	14	1,3
64,0	16,2	22	5,8
AVG			**2,27**

$$DScore = \frac{2 * (A \cap B)}{A + B} \tag{9}$$

In Eq. (9) '*A*' and '*B*' correspond to the ideal binary image and the binary image obtained from the algorithm respectively (Al-Shamri 2014). After the intersection operation between images *A* and *B*, their components are added together to obtain a single value. In the sum between *A* and *B*, first the components of each image are added together and then the two images are summed. Tables 3-4 shows the quality in the segmentation of several tests.

Table 5 shows the results in millimeters of carbonation depth in some database images compared to the results reported in the theory.

5. Conclusions

The determination of the carbonation depth is a highly

variable process, for which the implemented algorithms must work under all probable conditions. In this measure, once obtained the database with as many different samples as possible from various items found in specialized databases is possible to determine the main parameters that can affect the analysis of images, such as lighting, the size of concrete aggregates, the cut of the specimen, the type of specimen and the quality of the image.

From the above in the PDI algorithm, the computational cost is minimal (12 ms) but the illumination and the type of specimen significantly affect the process, since it was necessary to make modifications to the original algorithm for its operation in circular specimens to be adequate. Likewise, it is necessary to have good resolution images (from 400×400 pixels approximately) and avoid that they are blurred in order not to distort the results.

In the case of the IA algorithm, the computational cost was considerably increased by taking between 0.3s and 0.9s the analysis for each image, but since the carbonation analysis is not a mass process, the waiting time is adequate. On the other hand, the same arrangement of neural networks works without distinction of the type of specimen, even its operation is successful with specimens in poor condition due to the cut made for removal from the column. Besides, it was verified how the algorithm does not lose efficiency working with low-resolution images (less than 100×100 pixels), hence this was a measure to lower the computational cost.

Finally, the quality of the segmentation demonstrates that the implementation of an artificial intelligence algorithm in the determination of the carbonation depth obtains good results considering the high variability of this process. Additionally, the measured value of carbonation depth in millimeters has an average error of 2.27 mm, which supposes an adequate functionality of the algorithm emphasizing its objectivity, besides it is important to mention that the theoretical data come from measurements made by a human being and therefore lead to errors in their measurement. In some cases, it was even possible to detect some errors in the measurement of carbonation depth reported in the database.

Acknowledgments

This study has been supported by Vicerrectoría de Investigaciones de la Universidad Militar Nueva Granada under project number ING-2992, validity 2019.

References

Akcay, B., Sengul, C. and ali Tasdemir, M. (2016), "Fracture behavior and pore structure of concrete with metakaolin", *Adv. Concrete Constr.*, **4**(2), 71-88. https://doi.org/10.12989/acc.2016.4.2.071.

Al-Shamri, M.Y.H. (2014), "Power coefficient as a similarity measure for memory-based collaborative recommender systems", *Exp. Syst. Appl.*, **41**(13), 5680-5688. https://doi.org/10.1016/J.ESWA.2014.03.025.

Ali Hameed, A., Karlik, B., Salman, M.S. and Eleyan, G. (2019), "Robust adaptive learning approach to self-organizing maps", *Knowledge-Bas. Syst.*, **171**, 25-36. https://doi.org/10.1016/J.KNOSYS.2019.01.011.

Antonio, L., Mehul, B., Alessandro, O. and David, V. (2018), "The role of cognitive architectures in general artificial intelligence", *Cognit. Syst. Res.*, **48**, 1-3. https://doi.org/10.1016/J.COGSYS.2017.08.003.

Barros, J.A.O., Lourenco, L.A.P., Soltanzadeh, F. and Taheri, M. (2013), "Steel fibre reinforced concrete for elements failing in bending and in shear", *Adv. Concrete Constr.*, **1**(1), 1-27. https://doi.org/10.12989/acc.2013.1.1.001.

Cao, V. and Ronagh, H. (2013), "A model for damage analysis of concrete", *Adv. Concrete Constr.*, **1**(2), 187-200. https://doi.org/https://doi.org/10.12989/acc.2013.1.2.187.

Cheng, G., Liu, T., Wang, K. and Han, J. (2006), "Soft competitive learning and growing self-organizing neural networks for pattern classification", *2006 Eighth International Symposium on Symbolic and Numeric Algorithms for Scientific Computing*, 378-381. https://doi.org/10.1109/SYNASC.2006.68.

D'Urso, P., De Giovanni, L. and Massari, R. (2020), "Smoothed self-organizing map for robust clustering", *Inform. Sci.*, **512**, 381-401. https://doi.org/10.1016/J.INS.2019.06.038.

Emmanuel, R., Ahmed, L. and François, C. (2009), "A performance based approach for durability of concrete exposed to carbonation", *Constr. Build. Mater.*, **23**(1), 190-199. https://doi.org/10.1016/j.conbuildmat.2008.01.006.

Guedes, R., Sant Ana, R., Goncalves, L., Oliveira, A., Cardoso, B. and Garcez, A. (2018), "Assessment of the durability of grout submitted to accelerated carbonation test", *Constr. Build. Mater.*, **159**, 261-268. https://doi.org/10.1016/j.conbuildmat.2017.10.111.

Hikawa, H. and Maeda, Y. (2015), "Improved learning performance of hardware self-organizing map using a novel neighborhood function", *IEEE Tran. Neur. Network. Learn. Syst.*, **26**(11), 2861-2873. https://doi.org/10.1109/TNNLS.2015.2398932.

Choi, J.I., Lee, Y., Kim, Y.Y. and Lee, B.Y. (2017), "Image-processing technique to detect carbonation regions of concrete sprayed with a phenolphthalein solution", *Constr. Build. Mater.*, **154**, 451-461. https://doi.org/10.1016/j.conbuildmat.2017.07.205.

Jiang, C., Huang, Q., Gu, X. and Zhang, W. (2017), "Experimental investigation on carbonation in fatigue-damaged concrete", *Cement Concrete Res.*, **99**, 38-52. https://doi.org/10.1016/J.CEMCONRES.2017.04.019.

Khvorostukhina, E., L'vov, A. and Ivzhenko, S. (2017), "Performance improvements of a Kohonen self-organizing training algorithm", *2017 IEEE Conference of Russian Young Researchers in Electrical and Electronic Engineering (EIConRus)*, 456-458. https://doi.org/10.1109/EIConRus.2017.7910589.

Li, Z., Antao, T. and Yang, L. (2011), "Hand gesture recognition of sEMG based on modified Kohonen network", *2011 International Conference on Electronics, Communications and Control (ICECC)*, 1476-1479. https://doi.org/10.1109/ICECC.2011.6066477.

Liwu, M., Feng, Z., Min, D., Fei, J., Abir, A.T. and Aiguo, W. (2017), "Accelerated carbonation and performance of concrete made with steel slag as binding materials and aggregates", *Cement Concrete Compo.*, **83**, 138-145. https://doi.org/10.1016/j.cemconcomp.2017.07.018.

Makridakis, S. (2017), "The forthcoming Artificial Intelligence (AI) revolution: Its impact on society and firms", *Future.*, **90**, 46-60. https://doi.org/10.1016/J.FUTURES.2017.03.006.

Malerba, P.G., Sgambi, L., Ielmini, D. and Gotti, G. (2017), "Influence of corrosive phenomena on bearing capacity of RC and PC beams", *Adv. Concrete Constr.*, **5**(2), 117-143. https://doi.org/10.12989/acc.2017.5.2.117.

Moshfe, S., Khoei, A., Hadidi, K. and Mashoufi, B. (2010), "A fully programmable nano-watt analogue CMOS circuit for Gaussian functions", *2010 International Conference on*

Electronic Devices, Systems and Applications, 82-87. https://doi.org/10.1109/ICEDSA.2010.5503099.

Otsu, N. (1979), "A threshold selection method from gray-level histograms", *IEEE J. Mag.*, **9**(1), 62-66.

Papadakis, V.G. (2013), "Service life prediction of a reinforced concrete bridge exposed to chloride induced deterioration", *Adv. Concrete Constr.*, **1**(3), 201-213. https://doi.org/10.12989/acc2013.1.3.201.

Paul, S.C., Panda, B., Huang, Y., Garg, A. and Peng, X. (2018), "An empirical model design for evaluation and estimation of carbonation depth in concrete", *Measure.*, **124**, 205-210. https://doi.org/10.1016/J.MEASUREMENT.2018.04.033.

Pu, Q., Yao, Y., Wang, L., Shi, X., Luo, J. and Xie, Y. (2017), "The investigation of pH threshold value on the corrosion of steel reinforcement in concrete", *Comput. Concrete*, **19**(3), 257-262. https://doi.org/10.12989/cac.2017.19.3.257.

Revert, A., De Weerdt, K., Hombostei, K. and Geiker, M. (2018), "Carbonation-induced corrosion: Investigation of the corrosion onset", *Constr. Build. Mater.*, **162**, 847-856. https://doi.org/10.1016/j.conbuildmat.2017.12.066.

Rodriguez, G.R., Chaparro, W.A.A. and Aravena, R.V. (2014), "Software para el calculo de la velocidad de deterioro de los hormigones sometidos a carbonatacion", *Revista Latinoamericana de Metalurgia y Materiales*, **34**(1), 45-54.

Shibata, T., Fukuda, T. and Tanie, K. (1993), "Synthesis of fuzzy, artificial intelligence, neural networks, and genetic algorithm for hierarchical intelligent control-top-down and bottom-up hybrid method", *Proceedings of 1993 International Conference on Neural Networks*, Nagoya, Japan. https://doi.org/10.1109/IJCNN.1993.714321.

Taffese, W.Z., Sistonen, E. and Puttonen, J. (2015), "CaPrM: Carbonation prediction model for reinforced concrete using machine learning methods", *Constr. Build. Mater.*, **100**, 70-82. https://doi.org/10.1016/J.CONBUILDMAT.2015.09.058.

Tang, J., Wu, J., Zou, Z., Yue, A. and Mueller, A. (2018), "Influence of axial loading and carbonation age on the carbonation resistance of recycled aggregate concrete", *Constr. Build. Mater.*, **173**, 707-717. https://doi.org/10.1016/j.conbuildmat.2018.03.269.

Tetta, C.M. (1986), "AI: What's in it for you? Career pointers that may lead the intelligent to artificial intelligence", *IEEE Potent.*, **5**(3), 19-21. https://doi.org/10.1109/MP.1986.6500803.

Thada, V. and Vivek Jaglan, D. (2013), "Comparison of jaccard, dice, cosine similarity coefficient to find best fitness value for web retrieved documents using genetic algorithm", *Int. J. Innov. Eng. Technol.*, **2**(4), 202-205.

Wang, X.Y. and Lee, H.S. (2019), "Microstructure modeling of carbonation of metakaolin blended concrete", *Adv. Concrete Constr.*, **7**(3), 167-174. https://doi.org/https://doi.org/10.12989/acc.2019.7.3.167.

Wang, X.Y. and Yao, L. (2018), "Evaluation of carbonation service life of slag blended concrete considering climate changes", *Comput. Concrete*, **21**(4), 419-429. https://doi.org/https://doi.org/10.12989/cac.2018.21.4.419.

Woyciechowski, P. and Soko, J. (2017), "Self-terminated carbonation model as an useful support for durable concrete structure designing", *Struct. Eng. Mech.*, **63**(1), 55-64. https://doi.org/https://doi.org/10.12989/sem.2017.63.1.055.

Xu, H., Chen, Z., Li, S., Huang, W. and Ma, D. (2010), "Carbonation test study on low calcium fly ash concrete", *Appl. Mech. Mater.*, **34**, 327-331. https://doi.org/10.4028/www.scientific.net/AMM.34-35.327.

Zambon, I., Vidovic, A., Strauss, A., Matos, J. and Friedl, N. (2018), "Prediction of the remaining service life of existing concrete bridges in infrastructural networks based on carbonation and chloride ingress", *Smart Struct. Syst.*, **21**(3), 305-320. https://doi.org/https://doi.org/10.12989/sss.2018.21.3.305.

Zhou, X., Tu, X., Chen, A. and Wang, Y. (2019), "Numerical simulation approach for structural capacity of corroded reinforced concrete bridge", *Adv. Concrete Constr.*, **7**(1), 11-22. https://doi.org/https://doi.org/10.12989/acc.2019.7.1.011.

Zhu, W. and Francois, R. (2013), "Effect of corrosion pattern on the ductility of tensile reinforcement extracted from a 26-year-old corroded beam", *Adv. Concrete Constr.*, **1**(2), 121-136. https://doi.org/https://doi.org/10.12989/acc.2013.1.2.121.

Zhuguo, L. and Sha, L. (2018), "Carbonation resistance of fly ash and blast furnace slag based geopolymer concrete", *Constr. Build. Mater.*, **163**, 668-680. https://doi.org/10.1016/j.conbuildmat.2017.12.127.

CC